Acta Materialia 310 (2026) 122136

Contents lists available at ScienceDirect

Acta Materialia

journal homepage: www.elsevier.com/locate/actamat

Full length article

Mechanistic insights and activation stress analysis of deformation twinning in the Cantor multi-principal element alloy

Camila A. Teixeira [a], Ujjval Bansal [a,b], Guillaume Laplanche [c], Peter Gumbsch [a], Subin Lee [a,*], Christoph Kirchlechner [a]

[a] Institute for Applied Materials, Karlsruhe Institute of Technology (KIT), 76131, Karlsruhe, Germany
[b] Karlsruhe Nano Micro Facility (KNMFi), Karlsruhe Institute of Technology (KIT), 76344, Eggenstein-Leopoldshafen, Germany
[c] Institut für Werkstoffe, Ruhr-Universität Bochum, 44801, Bochum, Germany

ARTICLE INFO

Keywords:
Twinning mechanism
Twinning stress
Multi-principal element alloys (MPEAs)
Mechanical size effect
Micro-pillar compression

ABSTRACT

Deformation twinning is an important deformation mechanism for low stacking fault energy face-centered cubic (FCC) alloys including multi-principal element alloys, however, its underlying mechanism remains incompletely understood. In this work, we applied in situ scanning electron microscope (SEM) micro-pillar compression combined with microstructural investigations to gain insights into the fundamental mechanism of deformation twinning and its stress and/or strain dependence. Our findings reveal that the morphology of the deformation twins and the controlling mechanism vary with micro-pillar size. In sub-micron pillars, single-slip based twinning models like the three-layer model were predominant as confirmed by in situ deformation and *post-mortem* microstructural analyses. For pillar diameters above 3 μm, two different twin variants were observed including one formed by the three-layer mechanism, although the secondary twinning mechanism remains unclear. When the pillar diameter increased to 10 μm, the applied stresses was insufficient to activate deformation twinning, and dislocation slip became the dominant deformation mode. A quantitative stress analysis of pillars ranging from 0.14 μm to 10 μm in diameter showed a lower bound for twinning stress of approximately 130 MPa. Finally, size dependence investigations revealed no significant difference between twinning stress and full dislocation slip critical resolved shear stress. This not only proves that dislocation slip is a prerequisite for twinning, but also indicates that, above a threshold stress, twinning could be more strain rather than stress-dependent.

1. Introduction

Deformation twinning is a prominent deformation mechanism in face-centered cubic (FCC) alloys in general, but more specifically in multi-principal element alloys (MPEAs), such as the Cantor alloy and its derivatives, where it not only occurs at cryogenic temperature but also at room temperature [1–4]. Previous studies have shown that mechanical twinning contributes to strain hardening through the "dynamic Hall-Petch" effect, as the newly created twin interfaces become obstacles for the motion of dislocations and reduce their mean free path [2]. It is well understood that twin nucleation is favored in FCC alloys when they have a low stacking fault energy [5,6]. Twinning occurs when the crystal is subjected to external stress in particular crystallographic orientations [7–9] and to high-stress concentrations, and can also be affected by temperature and strain rate [10–13]. While high strain rates have shown to impact the thickness and nucleation of twin lamellae [12,13], high stress is believed to be crucial for twin formation. This has led to multiple attempts over the last decade to experimentally measure or theoretically predict the so-called twinning stress – the critical stress required to initiate deformation twinning [2,7,8,14–18]. Nevertheless, the fundamental mechanism for deformation twin formation and the physics behind this critical twinning stress remain subjects of ongoing debate.

Classically, twin nucleation and growth is explained by the successive emission of Shockley partial dislocations on adjacent {111} planes, producing a stacking fault in each plane and, consequently, leading to the formation of a micro-twin (or twin embryo) [9,19–21]. Although the general consensus is that twinning develops from dislocation plasticity [22], this mechanism represents an oversimplified view of twin nucleation – particularly regarding the mechanisms of twin growth, which remain incompletely understood. Consequently, more elaborated mechanisms have been proposed to explain both twin nucleation and

* Corresponding author.
E-mail address: subin.lee@kit.edu (S. Lee).

https://doi.org/10.1016/j.actamat.2026.122136
Received 11 August 2025; Received in revised form 18 February 2026; Accepted 15 March 2026
Available online 17 March 2026
1359-6454/© 2026 The Author(s). Published by Elsevier Inc. on behalf of Acta Materialia Inc. This is an open access article under the CC BY license (http://creativecommons.org/licenses/by/4.0/).

growth. In this work, we categorize these mechanisms into two main groups: single slip plane mechanisms [23–25] and multiple slip plane mechanisms [26–28] (see Table 1).

The term "single slip plane" refers to the models, in which deformation twinning evolves from dislocation plasticity solely on a single slip plane, as proposed in the three-layer and pole mechanisms [23–25]. In the three-layer mechanism, a twin source is formed by the reaction of co-planar dislocations gliding with different Burgers vectors, resulting in a three-layer stacking fault [25]. The pole mechanism proposes that a Shockley partial dislocation dissociates from the pole (Frank) dislocation and then glides away from it [23,24,29]. Through its repeated revolutions, it produces successive fault layers. Each cycle recreates the twin source, leading to the growth of the twin lamella [23,24,29].

The "multiple slip plane" case refers to the mechanisms, such as the two-layer [26], the stair-rod cross-slip [27], and the Cohen and Weertman mechanism [28], which require dislocation activities on multiple slip planes to form a twin source. For the multiple slip plane mechanisms, obstacles such as Lomer-Cottrell locks are typically required for dislocation pile-ups to form. These pile-ups then react with dislocations on different slip planes, dissociating into Shockley and Frank partial dislocations or Shockley and stair-rod dislocations, ultimately resulting in the development of a twin source [26–28].

Molecular dynamics (MD) simulations and in situ micro-mechanical scanning electron microscopy (SEM) or transmission electron microscopy (TEM) studies have attempted to validate the twinning mechanism in the derivatives of the Cantor alloy [17,30–34]. MD simulations in a CoCrNi alloy with 6–12 nm grain size have suggested two different twinning mechanisms: (i) the nucleation of leading partial dislocations from a grain boundary on adjacent {111} planes, forming a grain boundary twin source; and (ii) glide of two leading partial dislocations on different slip planes, whose interaction within the grain forms an intragranular twin source [32]. In situ SEM micro-pillar compression studies combined with MD simulations in a single crystal CoCrFeNi alloy suggested a twinning mechanism similar to the classical picture of consecutive motion of Shockley partial dislocations described above, however, the twinning process would initiate by the partial dislocation emission from initial dislocation sources or free surface sources [33]. A similar mechanism has also been reported for TWIP steel and Ga-As alloy micro-pillars [19,20,35]. In situ TEM investigations on CoCrNi have suggested that twinning could evolve from a reversible HCP-FCC

Table 1
Proposed twinning mechanisms classified in: single slip plane [9,23–25] and multiple slip plane mechanisms [26–28]. Note that, in the mechanism schematics section, gray is used to show the twinning slip system and bold is used to highlight the twinning Burgers vector.

Proposed mechanism		Mechanism schematic
Single slip plane	Copley and Kear: Partial dislocation mechanism	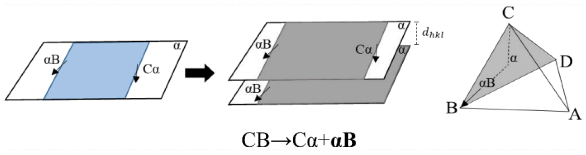 CB→Cα+**αB**
	Mahajan and Chin: Three-layer mechanism	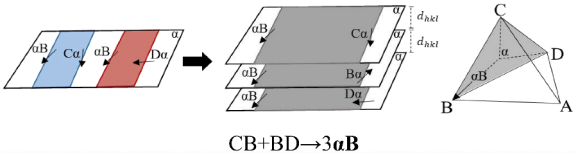 CB+BD→3**αB**
	Venables: Pole mechanism	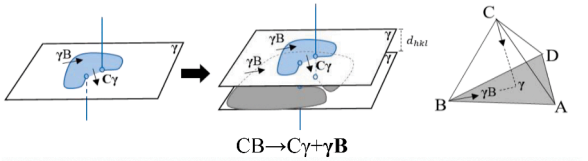 CB→Cγ+**γB**
Multiple slip plane	Narita and Takamura: Two-layer mechanism	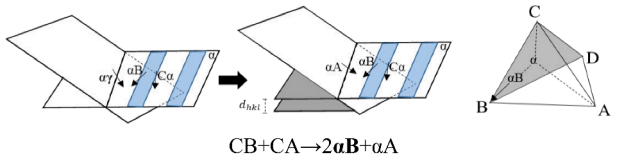 CB+CA→2**αB**+αA
	Fujita and Mori: Stair-rod cross-slip mechanism	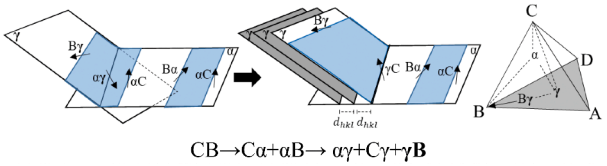 CB→Cα+αB→ αγ+Cγ+**γB**
	Cohen and Weertman mechanism	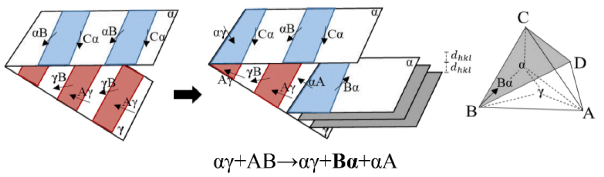 αγ+AB→αγ+**Bα**+αA

transformation [31]. However, it is well-known that both the critical resolved shear stress (CRSS) and the dominant deformation mode vary significantly with sample size at small scales, suggesting that the observed twinning mechanism may not be directly applicable to bulk specimens. This highlights the need for studies that bridge multiple length scales. However, to the best of authors' knowledge, there have been no experimental reports in the literature that systematically explore deformation twinning across a broad size range from nano to micron scale with a focus on the activated twinning mechanisms. Such studies would provide comprehensive insights into its fundamental underlying mechanisms and stress dependence, while also enabling an evaluation of the mechanical size effect on twinning stress and its estimation in the Cantor alloy.

This work aims to provide a more comprehensive understanding of the twinning mechanisms by combining quantitative stress analysis through *in situ* SEM micro-pillar compression tests, and advanced microstructure characterization. For this purpose, micro-pillars with diameters ranging from 0.14 μm to 10 μm were tested and the microstructures of the deformed pillars were thoroughly examined with a focus on mechanical twinning. By taking advantage of mechanical size effects, different levels of applied stress were achieved across the pillars with different diameter, enabling investigation of the stress dependence of activated twinning mechanisms. Furthermore, detailed twinning processes and twin morphologies were characterized through *post-mortem* microstructural analysis. This offers insight into the twinning mechanisms, since clear differences in the mechanical behavior and slip activity were observed as the micro-pillar sizes varied. Additionally, the mechanical size effect on twinning stress and a comparison with full dislocation slip were investigated.

2. Methodology

2.1. Sample preparation

The sample used in this work was provided by collaborators and the complete fabrication process description can be found in references [36, 37]. The Cantor alloy ($Co_{20}Cr_{20}Fe_{20}Mn_{20}Ni_{20}$ at. %) sample was arc melted under Ar atmosphere, using highly pure elements (99.95 wt. %), and cast into rod-shaped ingots in a water-cooled Cu mold. Measurements performed with an inductively coupled plasma optical emission spectrometry confirmed a chemical composition of 20.4 at. % Co, 19.7 at. % Cr, 20.3 at. % Fe, 19.2 at. % Mn and 20.4 at. % Ni (accuracy of 0.1 at. %) [36]. The 14 mm diameter as-cast ingots underwent (i) homogenization at 1473 K for 72 h in an evacuated glass tube followed by water quenching, (ii) diameter reduction to 6 mm by rotary swaging and (iii) annealing at 1273 K for 1 h. This resulted in a fully recrystallized microstructure with a grain size of approximately 60 μm. Before micro-pillar preparation, 1 mm thick pieces were cut with a diamond saw and underwent metallographic preparation, such as grinding followed by polishing, to guarantee a deformation-free top surface.

2.2. Micro-pillar fabrication

All the micro-pillars were cut from the center of a grain of the polycrystalline alloy. This resulted in single-crystalline micro-pillars without exception. Two different sets of micro-pillar orientations were tested, aiming at deformation twinning and full dislocation slip activation. The first subset was fabricated with a loading direction close to the lower left corner of the inverse pole figure (IPF), in other words, close to a ⟨100⟩ pole. In this orientation, the Schmid factor, *m*, for the leading

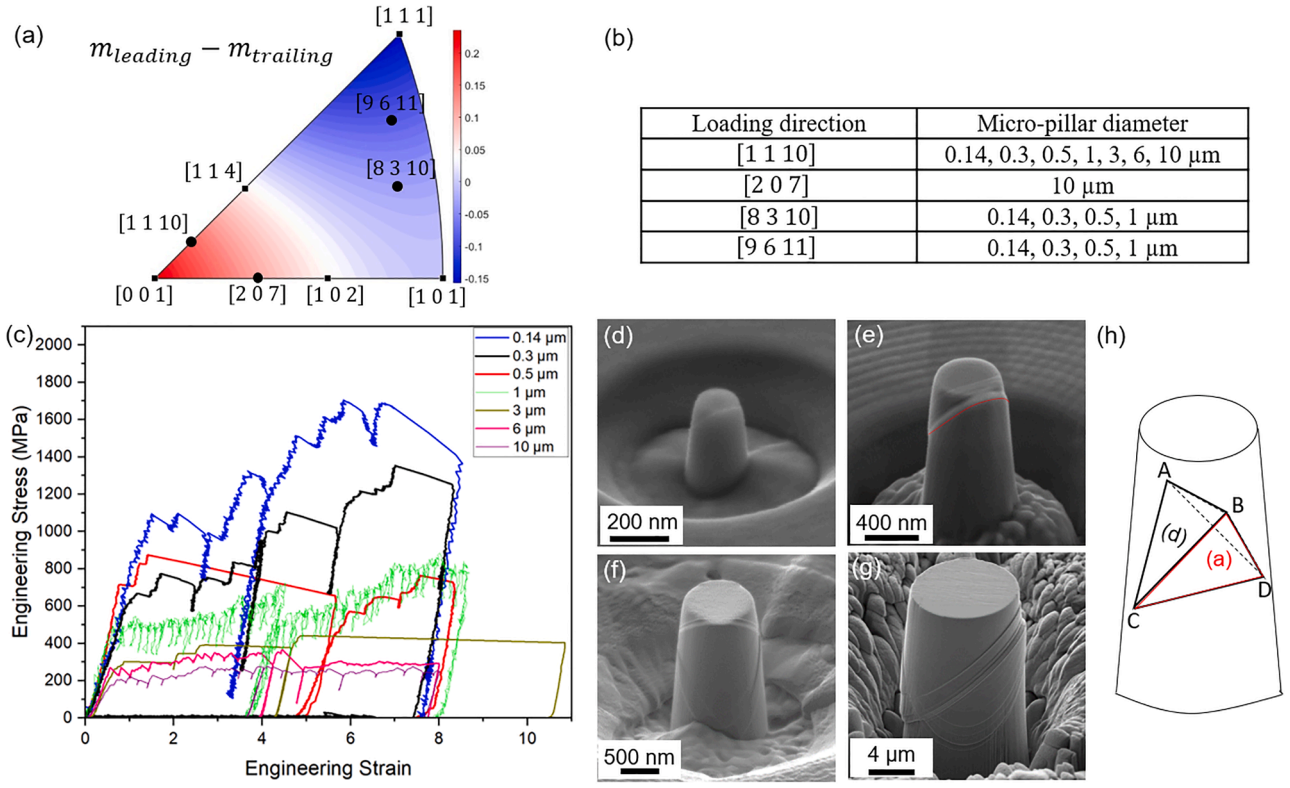

Loading direction	Micro-pillar diameter
[1 1 10]	0.14, 0.3, 0.5, 1, 3, 6, 10 μm
[2 0 7]	10 μm
[8 3 10]	0.14, 0.3, 0.5, 1 μm
[9 6 11]	0.14, 0.3, 0.5, 1 μm

Fig. 1. (a) IPF in Z-direction displaying the Schmid factor (m) difference between leading and trailing partial dislocation, including the chosen the micro-pillars crystallographic normal orientations (represented by the circle symbol). The $(1\bar{1}1)[112]$ (leading partial) and $(1\bar{1}1)[1\bar{2}1]$ (trailing partial) were considered for calculations. (b) Table of grain orientations as loading directions and diameters of the pillars fabricated inside the grains. (c) Representative engineering stress-strain curves of micro-pillars for each diameter. *Post-mortem* SEM secondary electron images of micro-pillars with diameters of (d) 0.14 μm, (e) 0.5 μm, (f) 1 μm, and (g) 10 μm. (h) Schematic representation of the Thompson tetrahedron oriented for a loading direction close to ⟨1 1 10⟩. Please note that the orientation of the Thompson tetrahedron in (h) is only representative of the micro-pillars (d) and (e), as (f) and (g) have a different in-plane orientation.

partial dislocation is maximized, to favor deformation twinning under compression (see Fig. 1(a) and (b)). The second subset of micro-pillars was fabricated with loading directions of [8 3 10] and [9 6 11] to favor full dislocation slip (see Fig. 1(a) and (b)). In this case, pillars with diameter up to 1 μm were milled, as above that diameter the mechanical data was previously reported in literature [42].

Electron back-scattered diffraction (EBSD) analyses were carried out with a Symmetry S2 (Oxford Instruments, United Kingdom) at an acceleration voltage of 20 kV and a current of 8 nA in a focused ion beam - scanning electron microscope (FIB-SEM) dual beam station (Crossbeam 550 L, Zeiss, Germany). Micro-pillars were machined using the same FIB (Crossbeam 550 L, Zeiss, Germany) with Ga^+ ions, an acceleration voltage of 30 kV and currents varying from 65 nA, for coarse milling, to 10 pA, for fine milling, according to the pillar size (see Supplementary Table S1 for more details). The diameters of the pillars oriented for twinning ranged from 0.14 μm to 10 μm and the diameters of those oriented for full dislocation slip ranged from 0.14 μm to 1 μm (Fig. 1(b)). A diameter-to-height ratio of 1:2–3 was maintained for all pillars to avoid elastic buckling. At least three micro-pillars were tested for each diameter.

For the micro-pillars oriented for deformation twinning, the loading axis – equivalent to the pillar normal direction – deviated by less than 5 degrees from [1 1 10] (see Supplementary Fig. S1 for more details), except for one 10-μm pillar which was cut from a [2 0 7] oriented grain (see Fig. 1(a) and (b)). However, please note that the micro-pillars may appear with different viewing directions in SEM imaging, as they were fabricated from grains with different in-plane orientation, despite having similar normal orientations.

2.3. In situ micro-pillar compression

In situ micro-pillar compression tests were performed in an SEM (Merlin Gemini II, Zeiss, Germany) using a Hysitron PI89 SEM Picoindenter (Bruker, USA) with two different load transducers with different stiffness: one with a maximum force of 0.5 N and noise floor of 5 μN, and another with a maximum load of 10 mN and noise floor of 0.4 μN. The transducer change was necessary due to the low forces expected for micro-pillars with sizes below 0.5 μm. The indenter was equipped with a diamond flat punch tip (Synthon-MDP AG, Switzerland) with diameters ranging from 2 μm to 20 μm, depending on the micro-pillar size. All tests were performed in displacement-control mode with a strain rate of 10^{-2} s^{-1} and a maximum strain of 8 %. The yield stress ($\sigma_{2\%}$) was determined using a 2 % plastic strain offset with unloading slope. In case of micro-pillars, yield stresses are typically computed at 1 % or 2 % plastic strain offset, instead of 0.2 %, as the initial elastic response of a micro-pillar might be influenced by misalignments between tip and the micro-pillar, which are accommodated at low strains [38]. Then, CRSS was calculated as $\tau_{2\%} = \sigma_{2\%} \cdot m$, where m is the Schmid factor of the activated slip system, determined by the SEM slip trace analysis and EBSD orientation analysis.

2.4. Post-mortem analyses

Post-mortem analyses were performed to detect the activation of deformation twinning and validate its mechanisms, which include (i) SEM imaging for slip trace analysis, (ii) EBSD analyses on micro-pillars top surfaces, (iii) back-scattered electron (BSE) imaging on FIB cross-section, and, in selected cases, (iv) TEM analyses. *Post-mortem* SEM imaging was performed with an acceleration voltage varying from 1 kV to 5 kV and a current from 130 pA to 500 pA. EBSD analyses were performed by varying the acceleration voltage from 20 kV to 30 kV and the current from 2 nA to 8 nA, to obtain the optimum contrast to resolve nanoscale twin lamellae. Prior to BSE imaging, the cross-section was FIB-milled to approximately one-third to half the micro-pillar diameter using FIB-SEM at an acceleration voltage of 30 kV. Depending on the pillar size, coarse milling was performed with a current of 1.5 nA (submicron pillars coarse step was skipped) followed by a polishing step with 50 pA to 10 pA. For TEM analyses, one micro-pillar for each diameter from 1 μm to 10 μm was prepared. The TEM lamellae were prepared using the same FIB-SEM, employing an acceleration voltage of 30 kV, with ion beam currents starting at 300 pA and finishing with fine polishing at 2 kV and beam current of 10 pA. TEM bright-field (BF) and dark-field (DF) micrographs were acquired at 300 kV (Themis 300, Probe aberration-corrected, Thermo Fisher Scientific, United States).

3. Results

3.1. In situ micro-pillar compression

The mechanical response of the micro-pillars showed typical features of a small-scale mechanical size effect [38], i.e. an increase in flow stress as well as a stochastic stress-strain response as the pillar diameter decreased (Fig. 1(c)). The usage of the high-resolution load transducer for micro-pillars with a diameter below 0.5 μm led to strain bursts instead of load drops (Fig. 1(c)), expected due to the pronounced intrinsic compliance of the low load transducer. Note that we limit the interpretation of mechanical data either to the first yield point causing a strain burst or to the flow stress at 2 % plastic strain, depending on whether the first strain burst surpassed the defined offset strain.

Given that the compression direction was predominantly aligned with ⟨1 1 10⟩ orientation (close to ⟨0 0 1⟩), the calculated Schmid factors, m, are similar or nearly identical for eight slip systems, and for four twinning systems, i.e. multiple slip is expected in all cases. However, *post-mortem* SEM imaging revealed that, for the submicron pillars, only one slip plane was activated during compression, meanwhile, activation of multiple slip planes was observed in larger micro-pillars (Fig. 1(d)-(g)). When a single slip plane was activated (Fig. 1(d) and 1(e)), the corresponding plane was identified as $(1\bar{1}1)$ by *post-mortem* slip trace analyses. Note that $(1\bar{1}1)$ is the plane (BCD) in the Thompson notation (see Fig. 1(h)), which is opposite to the corner A and will be further referred to as plane (*a*). This way, the plane (ACD), which is opposite to the B corner, will be referred to as plane (b) and so forth, following the Thompson notations. In the cases where two slip systems were activated, e.g. the 1 μm diameter micro-pillars (Fig. 1(f)), the activated slip planes were (*a*) and (*b*). In micro-pillars larger than 3 μm, all expected {111} slip planes were observed, similarly to the representative case of the 10 μm pillar (Fig. 1(g)). Furthermore, the slip direction was also analyzed using the *post-mortem* top and side view SEM images, as will be discussed in the following section.

The results for the micro-pillars oriented for full dislocation slip (compression axes parallel to [9 6 11] and [8 3 10], close to [111]) showed similar behavior in terms of an increase of flow stress with a decrease in pillar diameter, as typically observed in small-scale mechanics due to the size effect. These engineering stress vs. strain curve are presented as Supplementary materials (see Fig. S2 and Table S2) and the corresponding CRSS are included in the discussion.

3.2. Onset of deformation twinning

To confirm the occurrence or absence of deformation twinning, three different characterization techniques were applied (Fig. 2). EBSD analyses of all micro-pillar top surfaces (Fig. 2(a) and (b)) were performed first, as no further sample preparation was required. As can be seen from Fig. 2(b), a change in crystallographic orientation was observed on the IPF map in Z axis (IPF-Z), which was further evidenced by the 60-degree misorientation (twin-matrix) and a shared common pole (corresponding to the twin plane) on the (111) pole figure (PF) of the twinned region and matrix (see further pieces of evidence in Fig. S3 of the Supplementary materials). Additional EBSD analyses confirmed the presence of deformation twins in 6 out of 10 micro-pillars with diameters ranging from 1 μm to 6 μm. However, due to its limited spatial resolution, EBSD

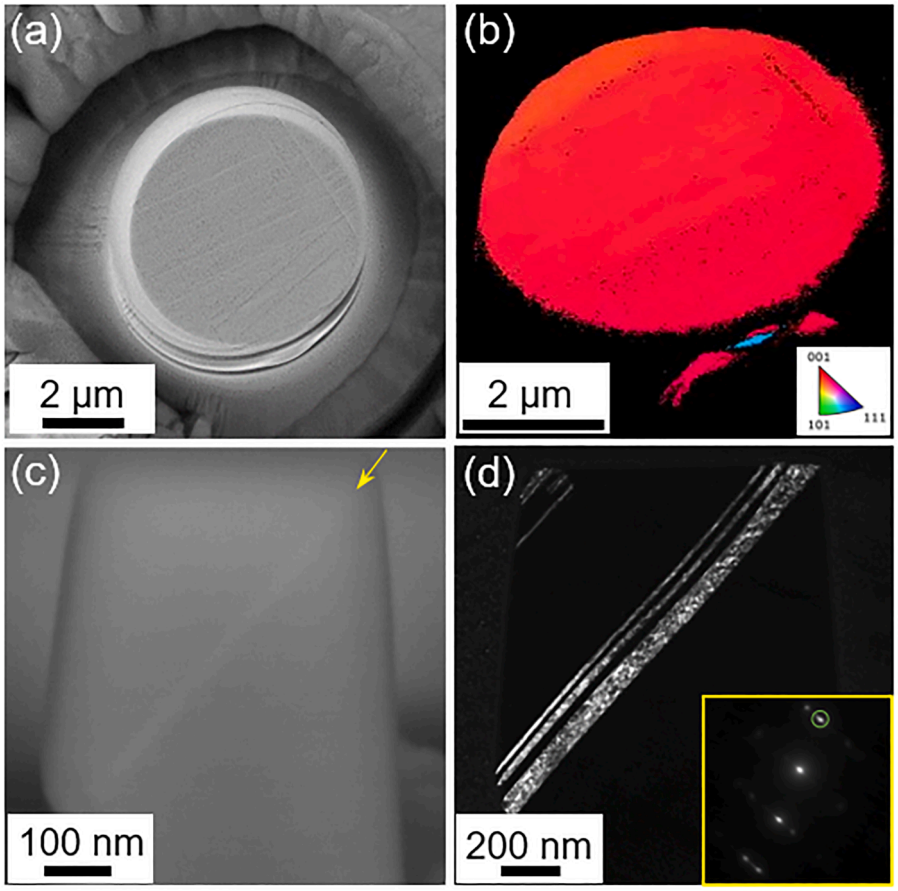

Fig. 2. Different microstructure analysis techniques used to confirm the activation of deformation twinning. (a) Slip direction analysis via SEM secondary electron imaging from the pillar top view direction. (b) EBSD IPF-Z map of the pillar top surface where the small blue region in the lower right corner corresponds to a twin lamella. (c) BSE image of a pillar cross section where the yellow arrow marks a twin lamella, and (d) TEM DF image obtained using the circled diffraction spot of the selected area diffraction pattern shown in the inset.

may miss nanotwins, and since it is only sensitive to deformation twins that intersect the top surface, it may also miss sub-surface twins. To confirm or rule out twinning in the sub-surface region, extensive investigations were conducted using BSE imaging on cross-sections and TEM of FIB lamellae.

In BSE cross-section images (e.g. Fig. 2(c)), twin lamellae were observed mainly in submicron pillars. Indeed, the presence of twin lamellae was confirmed in 10 out of 12 micro-pillars with diameters between 0.14 μm and 1 μm, but this technique was not successful in larger 3 μm and 6 μm sized pillars, where deformation twins were too fine to be resolved by BSE imaging. For these particular cases, FIB lamellae were lifted out from the pillars followed by TEM analyses, which confirmed the activation of deformation twinning, e.g. see the TEM BF and DF micrographs with a ⟨011⟩ zone axis in Fig. 2(d). Overall, deformation twinning was confirmed in 10 out of 12 micro-pillars with diameters below 3 μm, only in 3 out of 7 pillars for diameters ranging from 3 μm to 6 μm, while no deformation twins were observed in the 10-μm pillars (see Fig. 3).

In the micro-pillars which showed deformation twinning, the sub-micrometer pillars exhibited single slip activation only, while larger pillars predominantly showed multiple slip activation as summarized in Fig. 3. This specificity may help to identify the twinning mechanism, which will be discussed in detail in Section 4.

The CRSS-values were calculated with the highest Schmid factor, m, for the activated twinning system (i.e. twinning partial dislocation) for micro-pillars between 0.14 μm to 6 μm (see Figs. 3 and 4). This value is given even for the pillars where twinning was not observed. For the 10 μm micro-pillars, which showed multi-slip, the highest m of full dislocation slip was considered. In the following section, a detailed

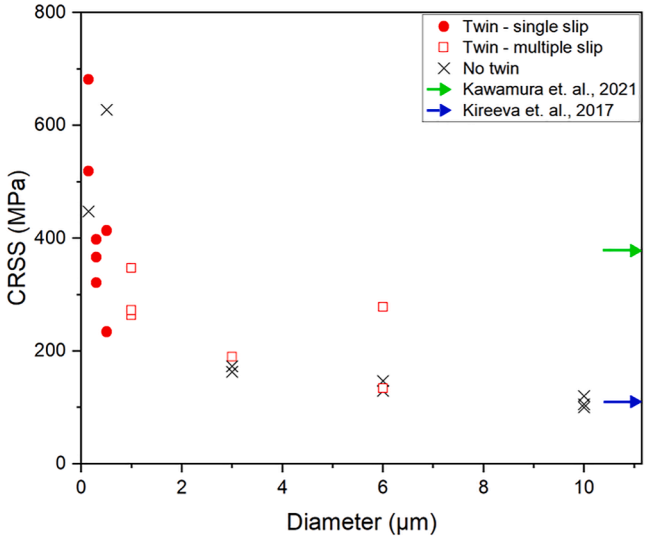

Fig. 3. Effect of pillar diameter on CRSS. The presence or absence of deformation twinning is highlighted with red symbols and black crosses, respectively. The activation of a single slip plane is marked by red dots, while multiple slip planes were detected otherwise. Lower and upper bounds of the twinning stress from the literature [39,40] are shown with arrows.

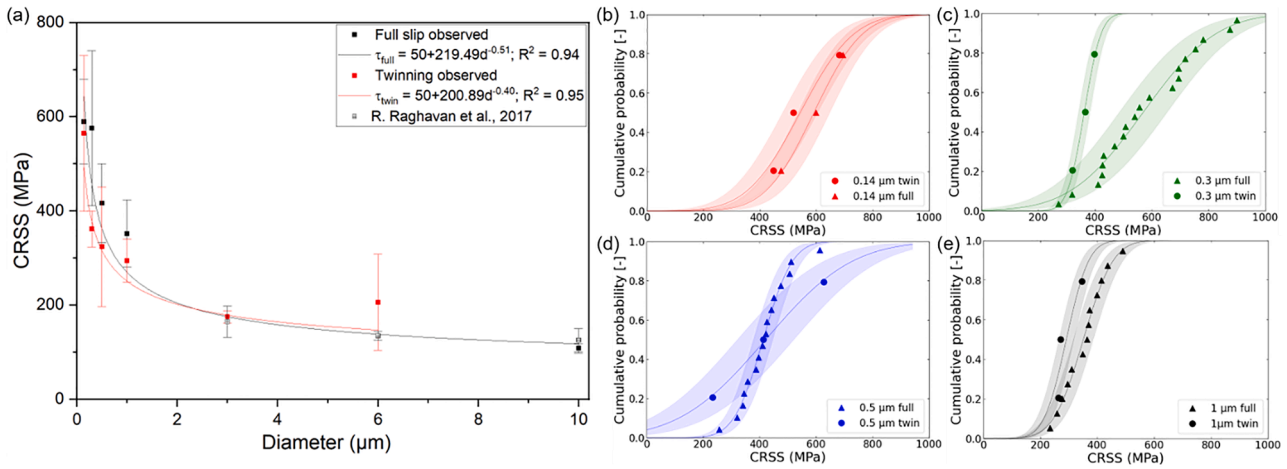

Fig. 4. (a) Mechanical size effect comparison plot between micro-pillars in which deformation twinning and full dislocation slip were observed. Note that for full dislocation slip 0.14 μm to 1 μm CRSS data are presented in the Supplementary materials and 3 μm, 6 μm and 10 μm CRSS data for full dislocation slip were taken from reference [42]; and 0.5 μm and 1 μm CRSS data for deformation twinning was previously published in [48]. Individual cumulative probability plot for (b) 0.14 μm, (c) 0.3 μm, (d) 0.5 μm and (e) 1 μm diameter micro-pillars.

analysis of the twinning stress is presented.

3.3. Twinning stress and mechanical size effect

To further understand the twinning mechanism, an analysis of the critical stresses for deformation twinning activation was performed. For the 10 μm pillar, the applied stresses appeared insufficient for twinning. This enabled the estimation of the twinning stress, determined by considering the lowest CRSS value of the micro-pillar that exhibited deformation twinning in the *post-mortem* analyses (Fig. 4), which was found to be approximately 130 MPa. The twinning stress of the Cantor alloy has been reported in the literature solely for interrupted mechanical testing in bulk. The value varies depending on grain size or, for single crystals, their crystallographic orientation [2,7,15,39–41]. The twinning stress estimated in our work is at the lower end of the reported range of 110 MPa to 378 MPa (Fig. 3) [2,7,15,39–41].

Additionally, the mechanical size effect on CRSS for deformation twinning and full dislocation slip was analyzed (see Fig. 4). Note that the mechanical data for micro-pillars with diameters of 3 μm, 6 μm, and 10 μm oriented for full dislocation slip were taken from reference [42]. The size scale power-law relationship [43] used for fitting is:

$$\tau_{2\%} = \tau_{bulk} + kD^{-n} \quad (1)$$

where D is the micro-pillar diameter, n is the size scaling exponent, k is a fitting parameter and τ_{bulk} is the bulk shear stress which was reported in the literature as 50.4 ± 2.0 MPa [44].

The fitting results indicate a slightly smaller size scaling exponent of twinning compared to full dislocation slip, suggesting that twinning stress could be less sensitive to a size change. The size exponent fitted was 0.40 ± 0.04 for deformation twinning and 0.51 ± 0.04 for full dislocation slip, which for the latter case is similar to previously reported in the literature [44]. Note that the error bars in Fig. 4(a) are standard deviations and the error on the size exponent was determined by the standard error scaled with the square root of reduced Chi-square. Overall, the size exponents for dislocation slip and deformation twinning are both smaller in the Cantor alloy than in FCC metals and binary alloys [45–47]. It has been suggested that in MPEAs, solid solution hardening or high lattice friction would be more dominant as strengthening mechanism and thus result in a lowersize exponent [33,42,44].

The smaller CRSS for deformation twinning compared to full dislocation slip, for sub-micron pillars, is surprising considering that prior dislocation reactions are required to form and activate twin sources (see Fig. 4(a)). To better interpret this size scaling difference, the CRSS results were further statistically investigated with cumulative probability plots (see Fig. 4(b)-(e)). The scatter bands indicate a 95 % confidence interval. The cumulative probability analysis was carried out only for micro-pillars with diameters ranging from 0.14 μm to 1 μm, which is the range where the CRSS for full dislocation slip exceeded the CRSS for deformation twinning. Although most of the analyzed data follows a consistent trend, a clear change in the distribution width is observed for the micro-pillars with a diameter of 0.3 μm: the mean CRSS of twinning was approximately 200 MPa lower than that of slip (see Fig. 4(c)). It suggests that this specific set of mechanical data may have contributed to the slightly reduced size effect calculated for deformation-twinning oriented micro-pillars. Therefore, in our study, the differences in the size scaling exponent for deformation twinning relative to full dislocation slip could be considered negligible.

In contrast, a less pronounced size dependency for deformation twinning, compared to full dislocation slip, has been previously reported for the CoCrFeNi MPEA micro-pillars with diameters ranging from 272 nm to 1253 nm [33]. This difference was attributed to dislocation starvation followed by nucleation of new dislocations from the free surfaces with additional straining, meanwhile, the twinning process would initiate by partial dislocation emission from pre-existent dislocations sources which would lead to a weaker size effect [33]. More detailed mechanisms will be discussed in Section 4.

3.4. Further slip system and TEM investigations

To explore the possible twinning mechanisms, further slip system analyses were performed for each near ⟨001⟩-oriented micro-pillar in combination with TEM investigations (Fig. 5). For sub-micron pillars, a single consistent slip plane was observed in all cases, therefore the 0.5 μm diameter was chosen for analyses as a representative example (see Fig. 5(a) and (b)). From both side and top views of this micro-pillar the slip plane (a) and a shear direction approximately parallel to DB (see Fig. 5(a) and (b)) were identified, which indicates that plastic deformation was mostly accommodated by slip of full ⟨110⟩-dislocations. BSE imaging of the 0.5 μm pillar cross-section (not shown here) revealed the presence of a twin lamella on the (*a*) plane on the same sample. This microstructural feature was also observed in other micro-pillars with diameters below 1 μm, where twinning was activated. In the case of 1 μm micro-pillars (Fig. 5(c)), two activated slip planes complicate the slip direction analysis from top-view SEM images. To circumvent this issue, TEM investigations were performed (see Fig. 5(e)). It was noted that the

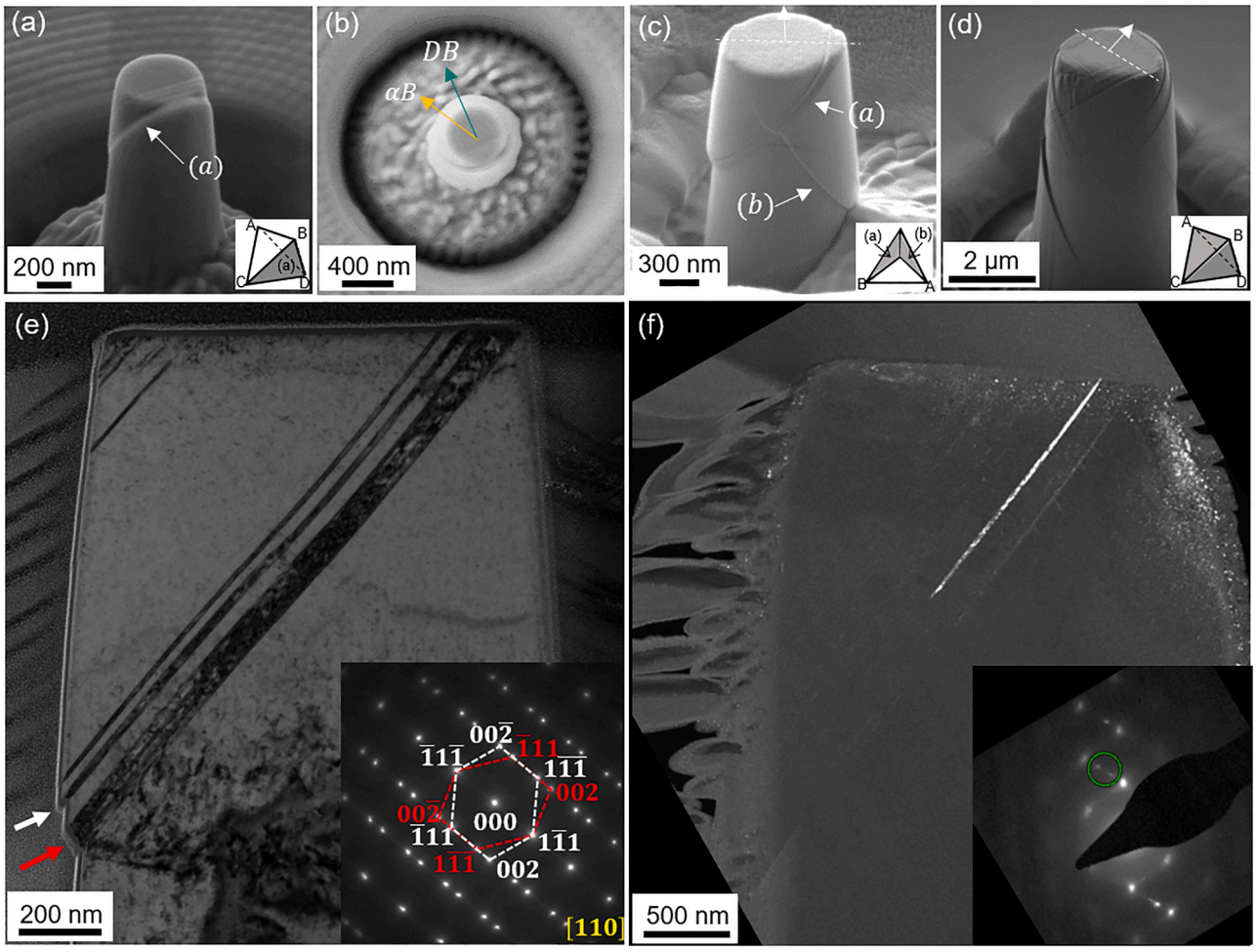

Fig. 5. Post-mortem SEM images of the (a) lateral and (b) top views of the 0.5 μm micro-pillar with a near <1 1 10>-loading axis (twinning orientation). Post-mortem SEM images of the (c) 1 μm and (d) 3 μm micro-pillars where the white dashed lines indicate from where TEM lamellae were taken. In the (e) TEM BF micrograph, twin lamellae parallel to the (111) plane are observed and twinning and dislocation slip steps on the lateral face of the pillar are highlighted by red and white arrows, respectively. A selected area diffraction pattern (SADP) taken along the [110]-zone axis and showing diffraction spots corresponding to the deformation twins is shown in the inset of (e). (f) Two-beam DF image obtained using the 110 diffracted spot marked with a green circle in the SADP, shown as an inset in the lower right corner.

twin lamella was formed on the (*a*) slip plane, and there was no clear evidence of slip/twin interactions, as no shearing of the twin lamellae was observed, although two slip planes were activated. Additionally, as highlighted by the red arrow in Fig. 5(e), an inclined surface step that is indicative of deformation twinning is observed, meanwhile, the white arrow highlights a sharp trace, which is indicative of dislocation slip. In the 3 μm micro-pillar case, not only multiple slip system activation but also different microstructural features in terms of twin nucleation, thickness, and lengthening were observed (Fig. 5(d) and (f)). TEM analyses revealed a single finer and shorter twin lamella, contrary to observations in smaller micro-pillars (Fig. 5(f)).

An additional twin morphology was observed for 3 μm and 6 μm pillars, which will be refered as the secondary twin and further discussed in Section 4.2, and the twin morphology observed in Fig. 5 will be refered as the primary twin.

4. Discussion

4.1. Mechanism for the primary twin

As previously mentioned, several mechanisms for twin nucleation have been proposed. However, given the (sub)micron size of the pillars, some of these mechanisms are unlikely to occur and could potentially be excluded. In bulk samples, for instance, prismatic sources and/or obstacles such as Lomer-Cottrell locks, essential components in models such as the pole or the two-layer mechanism [23,24,26–28,49,50], are more likely to exist than in small-scale samples with limited sample volume and dislocation population [19,51]. Taking the two-layer mechanism proposed by Narita and Takamura [26,49] as an example, either a Lomer-Cottrell lock should exist within the micro-pillar or two dislocations on different slip planes (hence two slip systems activated) should interact to form such immobile dislocations. Therefore, for the micro-pillars with diameters between 0.14 μm and 0.5 μm, where only a single slip plane was observed in all cases, such mechanisms are likely irrelevant because only very few dislocations are expected to be inside the pillars due to the low initial dislocation density of $4.6 \pm 1.8 \times 10^{12}$ m^{-2}, which was measured in the present study using electron channeling contrast imaging (Supplementary Fig. S4). In this scenario, only single-slip based twinning mechanisms remain plausible: (i) surface source nucleation of partial dislocations on adjacent ⟨111⟩-planes and (ii) the Mahajan and Chin three-layer mechanism [19,25,35].

Considering firstly the three-layer mechanism, this scenario would involve co-planar slip of full dislocations (with different Burgers vectors) to react and form a three-layer twin embryo. As observed for sub-micron pillars thus far (as shown for instance in Fig. 2(c)), the twin lamella appears to be nucleated from the top surface, more specifically, from the

top corner of the micro-pillar in contact with the indenter tip, where stress localization is most pronounced [52]. This feature was observed in several micro-pillars, and in fact enabled the twin lamella to be identified with top surface EBSD analyses. For the 1 μm micro-pillars, similarly the twin seems to nucleate from the top corner. The lack of interaction between slip traces (e.g. no shearing of the twin lamellae observed) could be an indication that no twin embryo was formed in the center of the micro-pillar, but rather at its top corner (Fig. 5(c) and (d)). Additionally, the sharp slip trace parallel to the twin observed in TEM DF images (white arrow in Fig. 5(c)) provided evidence of dislocation slip activity right at the newly formed twin (Fig. 5(c)). Such observations support the three-layer mechanism, i.e. a single slip plane mechanism, and undermine the multiple slip plane mechanisms. Furthermore, in addition to the activation of a single slip plane, the 0.5 μm micro-pillars exhibited evidence of full dislocation slip activity, as observed previously in *post-mortem* SEM analyses (Fig. 5(a) and (b)), which further supports the hypotheses of the three-layer mechanism. The three-layer twin nucleation requires co-planar slip to occur on a single slip plane where the full dislocations react to form a three-layer twin embryo through the reaction CB + DB→3αB, see Schmid factors in Table 2.

The second scenario, the nucleation of partial dislocations from surface sources cannot be entirely dismissed. FIB-induced damage can create surface defects which may serve as nucleation sites for dislocations [53–57]. The FIB-affected volume decreases with increasing micro-pillar size, it is most pronounced in the 0.14 μm diameter micro-pillars due to their higher surface-to-volume ratio. In this case, if a partial dislocation was to nucleate from a surface source, it would need to form a stacking fault extending approximately 0.2 μm (the distance spanned across a 0.14 μm diameter micro-pillar). For this to occur, a particular shear stress is required and could be estimated by the equation for the distance separation (d_s) between two partials proposed by [21], rearranging to calculate the external stress (τ_{zx}),

$$\tau_{zx} = \frac{2\gamma_{SF}}{b_p} - \frac{2(2-3\nu)Gb_p}{d_s[8\pi(1-\nu)]} \quad (2)$$

where γ_{SF} is the stacking fault energy, b_p is the partial dislocation Burgers vector, ν is the Poisson ratio and G is the shear modulus. Considering that for the Cantor alloy $G = 81$ GPa, $\nu = 0.25$ [58] and the γ_{SF} has been reported to be between 20 mJ/m^2 and 35 mJ/m^2 [8,10,15,39,41,59], the calculated lower bound for the external shear stress is 265 MPa, which is reached for micro-pillars between 0.14 μm and 1 μm diameter. However, for larger pillars, this stress is not reached, suggesting that surface nucleation of partial dislocations is not likely to occur in pillars larger than 1 μm. According to Eq. (2), the stacking fault energy is the major contributor to the necessary applied stress, and increasing the partial dislocation separation width, e.g. as micro-pillar size increases, has a negligible effect within the diameter range tested.

Nevertheless, surface nucleation does not seem to be the predominant source for twin nucleation in any case. If that was the case, deformation twinning should have been observed in various slip planes given the micro-pillars compression axis close to a ⟨1 1 10⟩ orientation, which results in similar m in multiple slip systems. Also, one could expect single extended stacking faults across the entire sample, which were never observed in our studies. In contrast, the same twin nucleation features from the micro-pillar top corner and in only one slip system were observed for the micro-pillars up to 1 μm diameter.

Table 2
Schmid factors of dislocations involved in the three-layer mechanism considering the 0.5 μm pillar actual orientation of [2 1 12] (see Supplementary Fig. 1 and Table S3 for details).

Dislocation type	Full dislocations		Leading partial dislocation
Burgers vector	CB	DB	αB
Schmid Factor	0.36	0.46	0.47

In larger micro-pillars (above 1 μm diameter), different features were observed as multiple slip systems were activated. For the 3 μm diameter micro-pillars, the twin lamella firstly seen seems to be nucleated from the top surface (Fig. 5(f)), similarly to smaller micro-pillars. However, a shorter and thinner twin lamella was noticed, which could suggest more contribution of dislocation slip to plastic deformation in larger micro-pillars. Furthermore, a different twin morphology was observed for pillars of 3 μm and 6 μm diameters and will be discussed in the following section.

4.2. Other twinning mechanisms?

Interestingly, compared to the previously observed twin morphology that starts from the top corner of the pillar, a different twin morphology was observed for micro-pillars with diameters of 3 μm and 6 μm (see Fig. 6). TEM DF micrographs under two-beam conditions show the presence of a secondary type of twins (Fig. 6(a) and (b)), which appear to be nucleated from the middle of an activated slip plane. They terminate in a rather equidistant manner from the slip plane and are present in the central region of the pillar, rather than being nucleated from its top surface as observed before. Note that the dark band to which the array of twins is connected is not a primary twin, but rather a slip trace, as confirmed by TEM electron diffraction analysis. A similar twin morphology was seen in the 6 μm pillar (Fig. 6(d) and (e)). In both cases, the determination of the exact twin plane was difficult due to the limited tilt angles in TEM investigation. However, the distance between the two spots, corresponding to the twin (insets of Fig. 6(a) and (d)), was ~9.5 nm^{-1}, suggesting that the reflections are from {111} planes.

In a multi-slip case, other twin mechanism, i.e. those that require dislocations of different slip planes to interact, are a possibility compared to the smaller micro-pillars as presented previously. Although the number of pre-existing dislocations in the 3 μm and 6 μm micro-pillars is expected to be greater, this number is still small given the low initial dislocation density of $4.6 \pm 1.8 \times 10^{12}$ m^{-2}. Therefore, the number of pre-existing dislocations is estimated to be approximately 30 and 150 in the 3 μm and 6 μm pillars, respectively. Please note that these dislocations are randomly distributed on planes, i.e. they are statistically stored dislocations. For a multi-slip mechanism to occur particular types of dislocations are required to be present, which might not be the case due to the small number of pre-existing dislocations. Alternatively, they need to be formed during compression. It should be mentioned that some pre-existing dislocations can escape through the free surface at low strains and, therefore, the likelihood of dislocations from different slip systems interacting to form a twin embryo can be considered low in small sample volumes. Thus we hypothesize that the interesting twin morphology in Fig. 6(b) and (e) forms by means of a different nucleation mechanism which is not based on pre-existing dislocations.

For instance, the secondary type of twins in Fig. 6(b) and (e) may have formed as a result of a de-twinning process on the dark band seen above them, from which they seemed to have nucleated. Instead of a reverse or pseudo reverse de-twinning mode (see [60,61]), in the first hypothesis we propose a simpler de-twinning process, which the same applied stress state is maintained and a complete return to the matrix crystallographic orientation is achieved. Once the primary twin lamella – the later dark band – is formed, it introduces twin boundaries within the previously single crystalline micro-pillar. Compatibility stresses could arise at the interface between the twinned region and matrix, as the difference in crystallographic orientation can lead to elastic and plastic anisotropy [62,63]. This causes the emission of the secondary twin. Subsequently, the stresses on the de-twinning Shockley (trailing) partials of the primary slip system could have been high enough to initiate de-twinning and complete the shift back to the matrix original orientation. The secondary twins, which terminate at the sharp interface to the primary twin, are limited in size due to the range of the compatibility stress remain.

A second possible scenario would be de-twinning caused by the

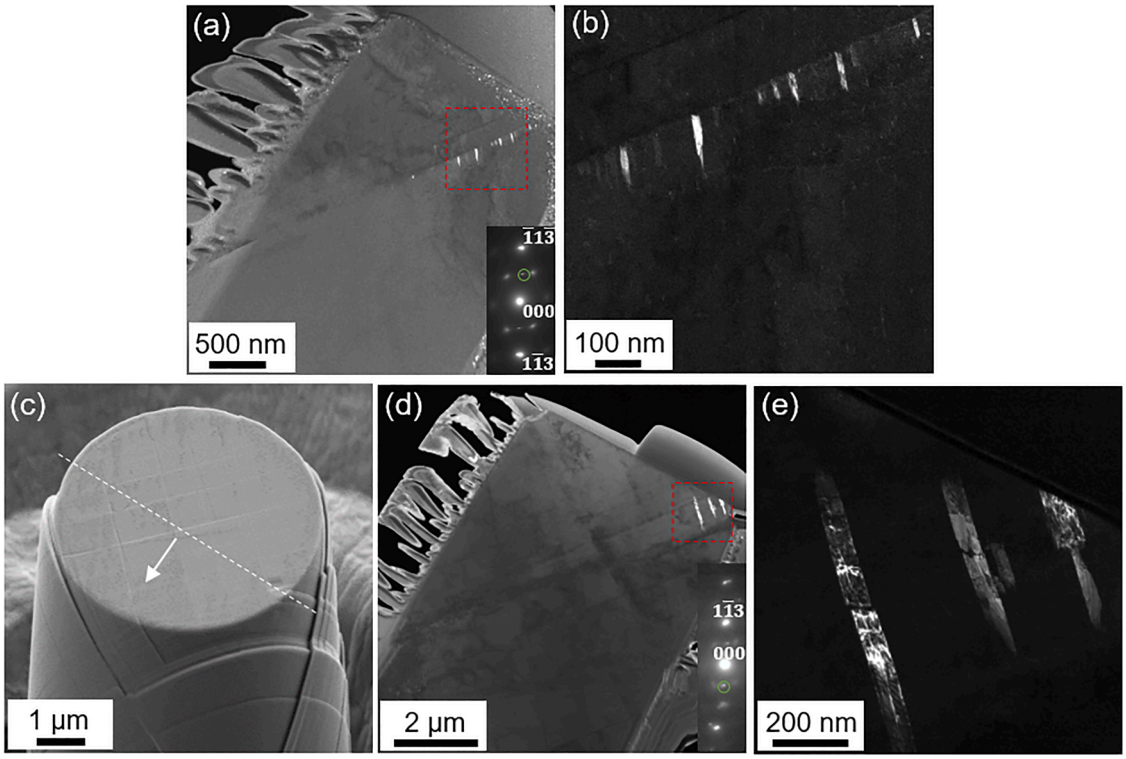

Fig. 6. Different twin morphology observed in 3 μm and 6 μm pillars. (a) TEM DF micrograph of a 3 μm diameter micro-pillar (same as that shown in Fig. 6(e)). A SADP in two-beam condition is shown as inset of (a). Here, the circled diffraction spot was selected to obtain the TEM DF micrographs. The region marked with a red frame in (a) is magnified in (b). (c) *Post mortem* SEM image of a 6 μm diameter micro-pillar where the white dashed line shows the region from where a TEM lamella was taken and the white arrow indicates the observation direction. (d) Corresponding TEM DF micrograph where the imaging conditions are shown in the inset. (e) Magnified micrograph from the red-framed region in (d).

interaction with dislocations of other slip planes. It is known that dislocation slip and twin boundary interaction might lead to either de-twinning or twin growth [64]. Supposing a leading partial dislocation (in a different slip plane) reaches the primary twin boundary, it can split into a stair-rod dislocation and another partial dislocation gliding in the twin plane [64]. This partial dislocation can lead to de-twinning of one atomic layer in one direction. If further dissociation of the stair-rod dislocation occurs, further de-twinning would be observed [64]. This process would be repeated until de-twinning of the entire lamellae occurs [64]. If during this process such sessile dislocation remains on the de-twinned region, it may react with other partial dislocations to form a twin embryo in a different slip plane [65], as proposed by Fujita and Mori in the stair-rod cross-slip mechanism [27] (see Table 1).

Nevertheless, it is difficult to determine the secondary twin mechanism, particularly in these multi-slip cases. Therefore, our results suggest that two different twin mechanisms occurred, however, the secondary twin mechanism remains unclear.

4.3. Sub-micron pillar CRSS difference in full slip and twinning

As discussed in Sections 4.1 and 4.2, deformation twinning nucleation evolves from dislocation slip activity. Therefore, one would expect that the CRSS for dislocation slip needs to be lower than the one for deformation twinning since dislocation slip is a prerequisite for twin source formation and additional processes are required to form twins. Surprisingly, the opposite was observed for micro-pillars with diameters below 3 μm, as CRSS for dislocation slip was higher than for deformation twinning (see Fig. 4(a)). This holds true even if the effective Schmid factor to calculate the CRSS for twinning would be considered a complex function of the co-planar full dislocations and leading partial dislocation, considering the three-layer mechanism. Note that the average CRSSs shown in Fig. 4(a) are the upper bound, as the leading partial dislocation Schmid factor was used, which is the highest in that slip plane. Hence, any complex function should not result in a higher CRSS.

Deformation twinning involves several key steps: (i) the nucleation of dislocations that initiate dislocation reactions, leading to the creation of a twin embryo, (ii) the formation of the twin embryo itself, and (iii) its activation. While the relative stress required for each step remains unclear, the negligible difference – or even lower CRSS – for micro-pillars deformed by twinning compared to those deformed by full slip suggests that the latter two factors may not play a dominant role at the micron and sub-micron scale. In other words, neither twin embryo formation nor its activation appears to require significant additional stress to the needed for the dislocation nucleation. Once the dislocations necessary for the twin source formation are present or nucleated, further twinning proceeds. This implies that deformation twinning above a certain threshold stress may be more strain-dependent than stress-dependent, requiring the presence and activation of specific dislocations in the sample to generate a twin embryo.

5. Conclusions

In this work, we applied in situ micro-pillar compression in an SEM to further understand the twinning mechanism in the CoCrFeMnNi Cantor HEA. In summary:

- Based on SEM and TEM investigations, single slip based twinning mechanisms like the three-layer twinning mechanism seem to be predominant in sub-micron pillars. The activation of a single slip plane and observations of full dislocation slip activity support the idea that the reaction of co-planar dislocations (with different Burgers vectots) could have led to the formation of a twin embryo.
- The difference in size scaling for dislocation slip and deformation twinning is negligible.

- The minimum CRSS for twinning was estimated as ~130 MPa based on the largest micro-pillars that exhibited deformation twins.
- In micro-pillars with diameters larger than 1 μm, an array of equi-distant and short secondary twins was observed. We hypothesized that their formation proceeded from a de-twinning process to accommodate stresses locally. While it is certain that two different twinning mechanisms occurred in large pillars, the mechanism in charge of the secondary twin type remains unclear.
- The formation of new deformation twins above a certain threshold stress could be strain-dependent rather than stress-dependent.

Data availability

Part of the data used in this work is available on: https://doi.org/10.5281/zenodo.14532279.

CRediT authorship contribution statement

Camila A. Teixeira: Writing – original draft, Visualization, Methodology, Investigation, Formal analysis, Data curation. **Ujjval Bansal:** Writing – review & editing, Investigation, Formal analysis. **Guillaume Laplanche:** Writing – review & editing, Formal analysis. **Peter Gumbsch:** Writing – review & editing, Formal analysis. **Subin Lee:** Writing – review & editing, Supervision, Methodology, Investigation, Formal analysis, Data curation. **Christoph Kirchlechner:** Writing – review & editing, Supervision, Methodology, Funding acquisition, Formal analysis, Conceptualization.

Declaration of competing interest

The authors declare that they have no known competing financial interests or personal relationships that could have appeared to influence the work reported in this paper.

Acknowledgments

Robert Bosch Stiftung and Helmholtz Program Materials Systems Engineering financial support is gratefully acknowledged by the authors. The authors also thank Reinhard Pippan and Jon Molina for the fruitful scientific discussions and Alexander Kauffmann for providing the samples used in this work. The Networking Grant granted by the Karlsruhe House of Young Scientist (KHYS) and the hosting period in IMDEA kindly accepted by Jon Molina is gratefully acknowledged. The TEM work was carried out with the support of the Kalrsruhe Nano Mcrio Facility (KNMFi), a Helmholtz Research Infrastructure at KIT.

Supplementary materials

Supplementary material associated with this article can be found, in the online version, at doi:10.1016/j.actamat.2026.122136.

References

[1] B. Gludovatz, A. Hohenwarter, D. Catoor, E.H. Chang, E.P. George, R.O. Ritchie, A fracture-resistant high-entropy alloy for cryogenic applications, Science 345 (2014) 1153–1158, https://doi.org/10.1126/science.1254581.
[2] G. Laplanche, A. Kostka, O.M. Horst, G. Eggeler, E.P. George, Microstructure evolution and critical stress for twinning in the CrMnFeCoNi high-entropy alloy, Acta Mater. 118 (2016) 152–163, https://doi.org/10.1016/j.actamat.2016.07.038.
[3] R.E. Kubilay, W.A. Curtin, Theory of twin strengthening in fcc high entropy alloys, Acta Mater. 216 (2021) 117119, https://doi.org/10.1016/j.actamat.2021.117119.
[4] E.P. George, W.A. Curtin, C.C. Tasan, High entropy alloys: a focused review of mechanical properties and deformation mechanisms, Acta Mater. 188 (2020) 435–474, https://doi.org/10.1016/j.actamat.2019.12.015.
[5] B. Gludovatz, A. Hohenwarter, K.V.S. Thurston, H. Bei, Z. Wu, E.P. George, R. O. Ritchie, Exceptional damage-tolerance of a medium-entropy alloy CrCoNi at cryogenic temperatures, Nat. Commun. 7 (2016) 1–8, https://doi.org/10.1038/ncomms10602.
[6] M. Beyramali Kivy, M.A. Zaeem, Generalized stacking fault energies, ductilities, and twinnabilities of CoCrFeNi-based face-centered cubic high entropy alloys, Scr. Mater. 139 (2017) 83–86, https://doi.org/10.1016/j.scriptamat.2017.06.014.
[7] W. Abuzaid, H. Sehitoglu, Critical resolved shear stress for slip and twin nucleation in single crystalline FeNiCoCrMn high entropy alloy, Mater. Charact. 129 (2017) 288–299, https://doi.org/10.1016/j.matchar.2017.05.014.
[8] I.V. Kireeva, Y.I. Chumlyakov, Z.V. Pobedennaya, I.V. Kuksgausen, I. Karaman, Orientation dependence of twinning in single crystalline CoCrFeMnNi high-entropy alloy, Mater. Sci. Eng. A 705 (2017) 176–181, https://doi.org/10.1016/j.msea.2017.08.065.
[9] S.M. Copley, B.H. Kear, The dependence of the width of a dissociated dislocation on dislocation velocity, Acta Metall. 16 (1968) 227–231.
[10] C. Wagner, G. Laplanche, Effects of stacking fault energy and temperature on grain boundary strengthening, intrinsic lattice strength and deformation mechanisms in CrMnFeCoNi high-entropy alloys with different Cr/Ni ratios, Acta Mater. 244 (2023) 118541, https://doi.org/10.1016/j.actamat.2022.118541.
[11] J.W. Christian, S. Mahajan, Deformation twinning, 1995. https://doi.org/10.1002/pssb.2221910204.
[12] G.H. Xiao, N.R. Tao, K. Lu, Effects of strain, strain rate and temperature on deformation twinning in a Cu-Zn alloy, Scr. Mater. 59 (2008) 975–978, https://doi.org/10.1016/j.scriptamat.2008.06.060.
[13] Y.L. Gong, C.E. Wen, X.X. Wu, S.Y. Ren, L.P. Cheng, X.K. Zhu, The influence of strain rate, deformation temperature and stacking fault energy on the mechanical properties of Cu alloys, Mater. Sci. Eng. A 583 (2013) 199–204, https://doi.org/10.1016/j.msea.2013.07.001.
[14] K.V.S. Thurston, A. Hohenwarter, G. Laplanche, E.P. George, B. Gludovatz, R. O. Ritchie, On the onset of deformation twinning in the CrFeMnCoNi high-entropy alloy using a novel tensile specimen geometry, Intermetallics 110 (2019) 106469, https://doi.org/10.1016/j.intermet.2019.04.012.
[15] C. Wagner, G. Laplanche, Effect of grain size on critical twinning stress and work hardening behavior in the equiatomic CrMnFeCoNi high-entropy alloy, Int. J. Plast. 166 (2023) 103651, https://doi.org/10.1016/j.ijplas.2023.103651.
[16] M. Schneider, J.P. Couzinié, A. Shalabi, F. Ibrahimkhel, A. Ferrari, F. Körmann, G. Laplanche, Effect of stacking fault energy on the thickness and density of annealing twins in recrystallized FCC medium and high-entropy alloys, Scr. Mater. 240 (2024), https://doi.org/10.1016/j.scriptamat.2023.115844.
[17] H. Huang, X. Li, Z. Dong, W. Li, S. Huang, D. Meng, X. Lai, T. Liu, S. Zhu, L. Vitos, Critical stress for twinning nucleation in CrCoNi-based medium and high entropy alloys, Acta Mater. 149 (2018) 388–396, https://doi.org/10.1016/j.actamat.2018.02.037.
[18] C. Wagner, E.P. George, G. Laplanche, Effects of grain size and stacking fault energy on twinning stresses of single-phase CrxMn20Fe20Co20Ni40-x high-entropy alloys, Acta Mater. 282 (2025) 120470, https://doi.org/10.1016/j.actamat.2024.120470.
[19] Z.Y. Liang, M.X. Huang, Deformation twinning in small-sized face-centred cubic single crystals: experiments and modelling, J. Mech. Phys. Solids 85 (2015) 128–142, https://doi.org/10.1016/j.jmps.2015.09.004.
[20] S.Z. Wu, H.W. Yen, M.X. Huang, A.H.W. Ngan, Deformation twinning in submicron and micron pillars of twinning-induced plasticity steel, Scr. Mater. 67 (2012) 641–644, https://doi.org/10.1016/j.scriptamat.2012.07.023.
[21] T.S. Byun, On the stress dependence of partial dislocation separation and deformation microstructure in austenitic stainless steels, Acta Mater. 51 (2003) 3063–3071, https://doi.org/10.1016/S1359-6454(03)00117-4.
[22] S. Mahajan, Critique of mechanisms of formation of deformation, annealing and growth twins: face-centered cubic metals and alloys, Scr. Mater. 68 (2013) 95–99, https://doi.org/10.1016/j.scriptamat.2012.09.011.
[23] J.A. Venables, Deformation twinning in face-centred cubic metals, Philos. Mag. 6 (1961) 379–396, https://doi.org/10.1080/14786436108235892.
[24] J.A. Venables, On dislocation pole models for twinning, Philos. Mag. 30 (1974) 1165–1169, https://doi.org/10.1080/14786437408207269.
[25] S. Mahajan, G.Y. Chin, Formation of deformation twins in f.c.c. crystals, Acta Metall. 21 (1973) 1353–1363.
[26] N. Narita, J. Takamura, Deformation twinning in silver- and copper-alloy crystals, Philos. Mag. 29 (1974) 1001–1028, https://doi.org/10.1080/14786437408226586.
[27] H. Fujita, T. Mori, A formation mechanism of mechanical twins in F.C.C. metals, Scr. Metall. 9 (1975) 631–636, https://doi.org/10.1016/0036-9748(75)90476-7.
[28] J.B. Cohen, J. Weertman, A dislocation model for twinning in f.c.c. metals, Acta Metall. 11 (1963) 996–998, https://doi.org/10.1016/0001-6160(63)90033-6.
[29] T.H. Lee, C.S. Oh, S.J. Kim, S. Takaki, Deformation twinning in high-nitrogen austenitic stainless steel, Acta Mater. 55 (2007) 3649–3662, https://doi.org/10.1016/j.actamat.2007.02.023.
[30] N.J. Liu, Z.J. Wang, J. Ding, M. Asta, R.O. Ritchie, B. Gan, E. Ma, Z.W. Shan, Origin of the high propensity for nanoscale deformation twins in CrCoNi medium-entropy alloy, J. Mater. Sci. Technol. 183 (2024) 63–71, https://doi.org/10.1016/j.jmst.2023.10.025.
[31] S. Chu, F. Zhang, D. Chen, M. Chen, P. Liu, Atomic-scale In situ observations of reversible phase transformation assisted twinning in a CrCoNi medium-entropy alloy, Nano Lett. 24 (2024) 3624–3630, https://doi.org/10.1021/acs.nanolett.3c04516.
[32] A. Gupta, W.R. Jian, S. Xu, I.J. Beyerlein, G.J. Tucker, On the deformation behavior of CoCrNi medium entropy alloys: unraveling mechanistic competition, Int. J. Plast. 159 (2022) 103442, https://doi.org/10.1016/j.ijplas.2022.103442.
[33] Q. Zhang, R. Huang, J. Jiang, T. Cao, Y. Zeng, J. Li, Y. Xue, X. Li, Size effects and plastic deformation mechanisms in single-crystalline CoCrFeNi micro/nanopillars,

J. Mech. Phys. Solids 162 (2022) 104853, https://doi.org/10.1016/j.jmps.2022.104853.
[34] L. Ding, A. Hilhorst, H. Idrissi, P.J. Jacques, Potential TRIP/TWIP coupled effects in equiatomic CrCoNi medium-entropy alloy, Acta Mater. 234 (2022) 118049, https://doi.org/10.1016/j.actamat.2022.118049.
[35] J. Michler, K. Wasmer, S. Meier, F. Östlund, K. Leifer, Plastic deformation of gallium arsenide micropillars under uniaxial compression at room temperature, Appl. Phys. Lett. (2007) 90, https://doi.org/10.1063/1.2432277.
[36] A.S. Tirunilai, J. Sas, K.P. Weiss, H. Chen, D.V. Szabó, S. Schlabach, S. Haas, D. Geissler, J. Freudenberger, M. Heilmaier, A. Kauffmann, Peculiarities of deformation of CoCrFeMnNi at cryogenic temperatures, J. Mater. Res. 33 (2018) 3287–3300, https://doi.org/10.1557/jmr.2018.252.
[37] K. Lu, A. Chauhan, A.S. Tirunilai, J. Freudenberger, A. Kauffmann, M. Heilmaier, J. Aktaa, Deformation mechanisms of CoCrFeMnNi high-entropy alloy under low-cycle-fatigue loading, Acta Mater. 215 (2021) 117089, https://doi.org/10.1016/j.actamat.2021.117089.
[38] G. Dehm, B.N. Jaya, R. Raghavan, C. Kirchlechner, Overview on micro- and nanomechanical testing: new insights in interface plasticity and fracture at small length scales, Acta Mater. 142 (2018) 248–282, https://doi.org/10.1016/j.actamat.2017.06.019.
[39] M. Kawamura, M. Asakura, N.L. Okamoto, K. Kishida, H. Inui, E.P. George, Plastic deformation of single crystals of the equiatomic Cr−Mn−Fe−Co−Ni high-entropy alloy in tension and compression from 10 K to 1273 K, Acta Mater. (2021) 203, https://doi.org/10.1016/j.actamat.2020.10.073.
[40] I.V. Kireeva, Y.I. Chumlyakov, Z.V. Pobedennaya, I.V. Kuksgausen, I. Karaman, Orientation dependence of twinning in single crystalline CoCrFeMnNi high-entropy alloy, Mater. Sci. Eng. A 705 (2017) 176–181, https://doi.org/10.1016/j.msea.2017.08.065.
[41] N.L. Okamoto, S. Fujimoto, Y. Kambara, M. Kawamura, Z.M.T. Chen, H. Matsunoshita, K. Tanaka, H. Inui, E.P. George, Size effect, critical resolved shear stress, stacking fault energy, and solid solution strengthening in the CrMnFeCoNi high-entropy alloy, Sci. Rep. 6 (2016) 1–10, https://doi.org/10.1038/srep35863.
[42] R. Raghavan, C. Kirchlechner, B.N. Jaya, M. Feuerbacher, G. Dehm, Mechanical size effects in a single crystalline equiatomic FeCrCoMnNi high entropy alloy, Scr. Mater. 129 (2017) 52–55, https://doi.org/10.1016/j.scriptamat.2016.10.026.
[43] R. Dou, B. Derby, A universal scaling law for the strength of metal micropillars and nanowires, Scr. Mater. 61 (2009) 524–527, https://doi.org/10.1016/j.scriptamat.2009.05.012.
[44] S. Lee, M.J. Duarte, M. Feuerbacher, R. Soler, C. Kirchlechner, C.H. Liebscher, S. H. Oh, G. Dehm, S. Lee, M.J. Duarte, M. Feuerbacher, R. Soler, Dislocation plasticity in FeCoCrMnNi high- entropy alloy : quantitative insights from in situ transmission electron microscopy deformation, Mater. Res. Lett. 8 (2020) 216–224, https://doi.org/10.1080/21663831.2020.1741469.
[45] D.M. Dimiduk, M.D. Uchic, T.A. Parthasarathy, Size-affected single-slip behavior of pure nickel microcrystals, Acta Mater. 53 (2005) 4065–4077, https://doi.org/10.1016/j.actamat.2005.05.023.
[46] W.S. Choi, B.C. De Cooman, S. Sandlöbes, D. Raabe, Size and orientation effects in partial dislocation-mediated deformation of twinning-induced plasticity steel micro-pillars, Acta Mater. 98 (2015) 391–404, https://doi.org/10.1016/j.actamat.2015.06.065.
[47] C.A. Volkert, E.T. Lilleodden, Size effects in the deformation of sub-micron Au columns, Philos. Mag. 86 (2006) 5567–5579, https://doi.org/10.1080/14786430600567739.
[48] C.A. Teixeira, S. Lee, C. Kirchlechner, Measuring the twinning stress at the micron scale: a comprehensive comparison of testing geometries, Mater. Charact. 217 (2024) 114314, https://doi.org/10.1016/j.matchar.2024.114314.
[49] N. Narita, J.I. Takamura, Twinning in f.c.c. and b.c.c. metals, Dislocat. Solids. 9 (1992) 135–169.
[50] A.H. Cottrell, B.A. Bilby, LX. A mechanism for the growth of deformation twins in crystals, Dublin Philos. Mag. J. Sci. 42 (1951) 573–581, https://doi.org/10.1080/14786445108561272.
[51] J.R. Greer, J.T.M. De Hosson, Plasticity in small-sized metallic systems: intrinsic versus extrinsic size effect, Prog. Mater. Sci. 56 (2011) 654–724, https://doi.org/10.1016/j.pmatsci.2011.01.005.
[52] A. Cornec, E. Lilleodden, Numerical analysis of micropillar compression behaviour and stress-strain curve estimation verified on glass fused silica, Mater. Today Commun. 33 (2022) 104971, https://doi.org/10.1016/j.mtcomm.2022.104971.
[53] S. Lee, J. Jeong, Y. Kim, S.M. Han, D. Kiener, S.H. Oh, FIB-induced dislocations in Al submicron pillars: annihilation by thermal annealing and effects on deformation behavior, Acta Mater. 110 (2016) 283–294, https://doi.org/10.1016/j.actamat.2016.03.017.
[54] Z.Y. Liang, J.T.M. De Hosson, M.X. Huang, Size effect on deformation twinning in face-centred cubic single crystals: experiments and modelling, Acta Mater. 129 (2017) 1–10, https://doi.org/10.1016/j.actamat.2017.02.063.
[55] S. Shim, H. Bei, M.K. Miller, G.M. Pharr, E.P. George, Effects of focused ion beam milling on the compressive behavior of directionally solidified micropillars and the nanoindentation response of an electropolished surface, Acta Mater. 57 (2009) 503–510, https://doi.org/10.1016/j.actamat.2008.09.033.
[56] L. Borasi, A. Slagter, A. Mortensen, C. Kirchlechner, On the preparation and mechanical testing of nano to micron-scale specimens, Acta Mater. (2024) 120394, https://doi.org/10.1016/j.actamat.2024.120394.
[57] S.H. Oh, M. Legros, D. Kiener, P. Gruber, G. Dehm, In situ TEM straining of single crystal Au films on polyimide: change of deformation mechanisms at the nanoscale, Acta Mater. 55 (2007) 5558–5571, https://doi.org/10.1016/j.actamat.2007.06.015.
[58] G. Laplanche, P. Gadaud, O. Horst, F. Otto, G. Eggeler, E.P. George, Temperature dependencies of the elastic moduli and thermal expansion coefficient of an equiatomic, single-phase CoCrFeMnNi high-entropy alloy, J. Alloys Compd. 623 (2015) 348–353, https://doi.org/10.1016/j.jallcom.2014.11.061.
[59] S.F. Liu, Y. Wu, H.T. Wang, J.Y. He, J.B. Liu, C.X. Chen, X.J. Liu, H. Wang, Z.P. Lu, Stacking fault energy of face-centered-cubic high entropy alloys, Intermetallics 93 (2018) 269–273, https://doi.org/10.1016/j.intermet.2017.10.004.
[60] M.S. Szczerba, S. Kopacz, M.J. Szczerba, On the reverse mode of fcc deformation twinning, Acta Mater. 60 (2012) 6413–6420, https://doi.org/10.1016/j.actamat.2012.08.028.
[61] M.J. Szczerba, S. Kopacz, M.S. Szczerba, Experimental studies on detwinning of face-centered cubic deformation twins, Acta Mater. 104 (2016) 52–61, https://doi.org/10.1016/j.actamat.2015.11.025.
[62] I. Tiba, T. Richeton, C. Motz, H. Vehoff, S. Berbenni, Incompatibility stresses at grain boundaries in Ni bicrystalline micropillars analyzed by an anisotropic model and slip activity, Acta Mater. 83 (2015) 227–238, https://doi.org/10.1016/j.actamat.2014.09.033.
[63] T. Richeton, I. Tiba, S. Berbenni, O. Bouaziz, Analytical expressions of incompatibility stresses at Σ3111 twin boundaries and consequences on single-slip promotion parallel to twin plane, Philos. Mag. 95 (2015) 12–31, https://doi.org/10.1080/14786435.2014.984787.
[64] Y.T. Zhu, X.L. Wu, X.Z. Liao, J. Narayan, L.J. Kecskés, S.N. Mathaudhu, Dislocation-twin interactions in nanocrystalline fcc metals, Acta Mater. 59 (2011) 812–821, https://doi.org/10.1016/j.actamat.2010.10.028.
[65] S. Picak, The role of stair-rod dislocations on the twinning and martensitic transformation in single crystalline NiCoCr, Scr. Mater. 258 (2025) 116522, https://doi.org/10.1016/j.scriptamat.2024.116522.